Received: 22 July 2021 | Revised: 18 October 2021 | Accepted: 28 November 2021

DOI: 10.1002/stc.2914

RESEARCH ARTICLE

WILEY

Particle filter-based hybrid damage prognosis considering measurement bias

Tianzhi Li[1] | **Claudio Sbarufatti**[1] | **Francesco Cadini**[1] | **Jian Chen**[2] | **Shenfang Yuan**[2]

[1]Department of Mechanical Engineering, Politecnico di Milano, Milano, via La Masa 1, 20156, Italy

[2]Research Center of Structural Health Monitoring and Prognosis, State Key Laboratory of Mechanics and Control of Mechanical Structures, Nanjing University of Aeronautics and Astronautics, Nanjing, China

Correspondence
Claudio Sbarufatti, Department of Mechanics, Polytechnic University of Milan, Milan, Italy.
Email: claudio.sbarufatti@polimi.it

Funding information
H2020 Marie Skłodowska-Curie Actions, Grant/Award Number: 859957; Horizon 2020

Summary

Hybrid methods combining physical knowledge and data-driven techniques have shown great potential for damage prognosis in structural health monitoring (SHM). Current practices consider the physics-based process and data-driven measurement equations to describe the damage evolution and the mapping between the damage state and the measurement, respectively. However, the bias between the measurements predicted by the data-driven equation and the sensor-based measurements obtained from any SHM system, arising from uncertainties like damage geometries and sensor placement or noise, can lead to inaccurate prognosis results. To improve the prognosis performance in case of bias, this paper adopts a methodology typically applied in sensor fault diagnosis and develops a new hybrid prognostic model with a bias parameter included in the measurement equation and the state vector. Particle filter (PF) serves as the estimation technique to identify the state and parameters relating to the damage as well as the bias parameter, and the remaining useful life (RUL) can be predicted by the physics-based process equation, with PF posterior estimates of the related parameters and state variables as an input. The experimental study of an aluminum lug structure subject to fatigue crack growth and equipped with a Lamb wave monitoring system demonstrates the improved estimation and prediction performances of the new prognostic model.

KEYWORDS

fault prognosis, hybrid model, Lamb wave, measurement bias, measurement equation, particle filter

1 | INTRODUCTION

Structural degradation is a phenomenon affecting the majority of engineering structures, which may lead to the occurrence of structural damage and eventually structural failure if not properly addressed. Regular inspection and maintenance should be carried out during the service life of a structure to ensure the structural safety, however often

incurring in high operative costs. In a predictive maintenance scenario, to simultaneously guarantee the safety at a reduced cost, inspection can be scheduled sufficiently before the structural damage reaches a critical level that may hamper the structural performance, which requires advanced prognostic techniques to predict the remaining useful life (RUL).

In the last decades, a great variety of damage prognosis techniques have been developed, depending on the availability of physics knowledge and data. From the perspective of how the prognostic models are formulated, they can be classified into physics-based,[1–3] data-driven,[4–6] and hybrid methods.[7–11] Physics-based methods utilize specific mechanistic knowledge and theories to formulate pure physics-based models, which describe the structural degradation phenomena and the links between the damage states and the SHM measurements. Data-driven methods, resorting to data-driven modeling techniques such as neural networks[4,6] and Markov chains,[5] attempt to use a large amount of data to build the relationship between the internal degradation behavior and the external observations. Hybrid methods, taken as a combination of the two above, usually consider the physics-based process and data-driven measurement equations to describe the damage evolution and the mapping between the damage state and the measurement, respectively.

The proper method (or model) is case-specific, as each type of method has its pros and cons.[12–14] A common belief is that, given the uncertainties arising from complex structural degradations, the environmental effects, and the sensor health conditions,[15,16] either the physics-based or the data-driven methods with sole deterministic models cannot provide an accurate prognostic result. A well-acknowledged strategy for both the physics-based[1–3] and data-driven methods[4–6] to improve their prognostic performance is to set the model parameters as unknown variables to be updated by a state estimation technique, such as the particle filter (PF) given its versatility for nonlinear and non-Gaussian problems. However, this strategy is not fully exploited in hybrid methods,[8,9,17] where the physics-based process equation is updated by setting its parameters as unknown variables to be estimated by PF, while the data-driven measurement equation is typically fixed.

Focusing on the latter, the relationship between the damage state and the measurement should probably vary in different specimens of the same structure[7] due to the uncertainties mentioned above. In practice, if the measurement equation describing the above relationship is built using both a data-driven modeling technique and the data from some specimens, then the bias between the measurements from a test specimen and those predicted by the measurement equation is unavoidable. In this context, the measurement equation that fails to be online updated or to take the bias into account will lead to inaccurate damage estimation[18] and prognosis[7] in case of large-level bias. Such a problem is investigated only in a few hybrid damage prognosis studies,[7,11,19] where either (i) the true damage state obtained by an additional measurement system is adopted to update the measurement equation at prescribed time instants[7,11] or (ii) all the parameters of both the process and measurement equations are set as unknown components to be estimated online,[19] strongly enhancing the algorithm adaptability to system deviations. However, on one hand, it is rarely possible to provide additional system observations of the true damage state, and on the other hand, it is always desired to limit to a minimum the parameters to be updated online for a robust algorithm convergence and to guarantee the state space full observability.

We anticipated that the bias between the sensor-based and the predicted measurements can be regarded as a typical sensor fault, which can be detected, localized, and identified by adding a bias parameter in both the measurement and process equations for estimation.[20,21] Moreover, leveraging on the little effect this bias can have on the estimation of other state components when accurately estimated by a state estimation technique, it has also been used for physics-based damage prognosis in An et al.,[22] where the bias is an error caused by the measurement system and is considered as a fixed parameter, but never in the hybrid damage prognosis framework so far, where the bias originating from multiple uncertainties can hardly be avoided and it is generally time varying.

This paper develops a new hybrid prognosis model that combines the approaches from sensor fault diagnosis and hybrid prognosis. The hybrid prognostic framework is based on a PF and it consists of three main steps. First, the measurement equation is built by a data-driven technique (i.e., polynomial fitting regression) with a bias parameter included to consider time variable discrepancies in consecutive tests, while the process equation considers the physical law describing damage evolution, and its state vector is augmented to include the damage state, the degradation law parameters, and the measurement bias. Then, the PF is used to estimate the damage state and model parameters. Finally, the future states and the RUL are estimated resorting to the process equation and the estimated damage state and parameters. The proposed prognostic framework is validated by an experimental activity, consisting of a fatigue crack growth in an aluminum structure, equipped with a Lamb wave measurement system.

The rest of this paper is organized as follows: Section 2 introduces the traditional and new models as well as the prognostic framework. The experimental validation is discussed in Section 3. Finally, Section 4 concludes this paper with a view toward future activities.

2 | DAMAGE PROGNOSIS FRAMEWORK

PF-based damage prognosis generally includes three main steps, namely, (i) formulating the prognostic model in a state space, (ii) estimating the unknown state variables using PF, and (iii) calculating the future state and RUL by taking the posterior PF estimates and the process equation into account. The hybrid damage prognosis framework taking the unknown bias into consideration is schematized in Figure 1, while details will be provided in the following paragraphs, where the differences with respect to the traditional version[8,9] are highlighted. Note: the variables b, $\boldsymbol{\theta}$, x, y, and the function $g(\cdot)$ will be introduced in Section 2.1.

2.1 | New prognostic model

Assume a discrete form of damage evolution model can be described as

$$x_k = f(x_{k-1}, \boldsymbol{\theta}), \tag{1}$$

where x is the damage state, $\boldsymbol{\theta}$ is a vector including the parameters governing the damage evolution, the subscript k is the discrete time step, and the function $f(\cdot)$ is usually a physical or semi-empirical law. The parameters $\boldsymbol{\theta}$ can vary in different specimens of the same structure due to the uncertainties in the damage evolution process; a deterministic evolution model may hardly provide accurate prognosis results. To overcome this problem, according to the common practices in PF-based prognosis, the parameters in $\boldsymbol{\theta}$ should also be taken as unknown variables to be online updated within the process equation:[8,17]

$$\boldsymbol{z}_k = \begin{bmatrix} \boldsymbol{\theta}_k \\ x_k \end{bmatrix} = \begin{bmatrix} \boldsymbol{\theta}_{k-1} + \boldsymbol{\omega}_{\theta,k} \\ f(x_{k-1}, \boldsymbol{\theta}_k, \omega_k) \end{bmatrix}, \tag{2}$$

where $\boldsymbol{z}$ is the state vector with both the damage state x and the model parameters $\boldsymbol{\theta}$ included, ω and $\boldsymbol{\omega}_\theta$ are the process noises for the damage state and the parameters, respectively.

Given the difficulties in directly measuring the damage state, many PF-based damage prognosis investigations[8,17] have the unknown damage state inferred from indirect observations y, related each other through a measurement equation $g(\cdot)$. The traditional state space model in hybrid damage prognosis can be formulated as follows.[8,17]

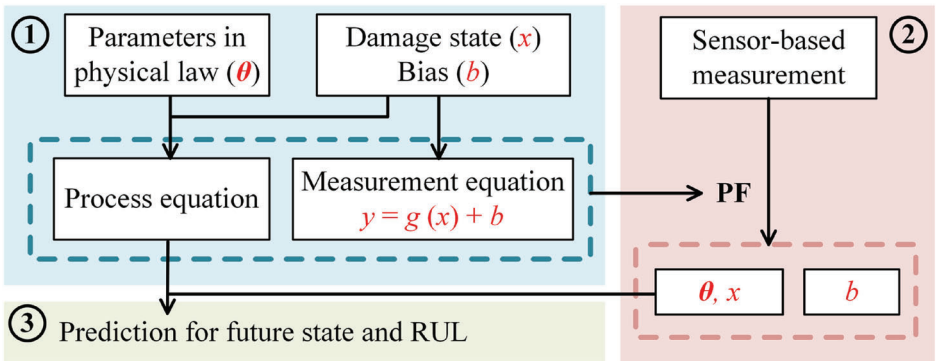

FIGURE 1 Hybrid damage prognosis framework

$$\begin{cases} \boldsymbol{z}_k = \begin{bmatrix} \boldsymbol{\theta}_k \\ x_k \end{bmatrix} = \begin{bmatrix} \boldsymbol{\theta}_{k-1} + \boldsymbol{\omega}_{\theta,k} \\ f(x_{k-1}, \boldsymbol{\theta}_k, \omega_k) \end{bmatrix}, \\ y_k = g(x_k) + \nu_k \end{cases} \tag{3}$$

where the data-driven function $g(\cdot)$ describes the relationship between the damage state x and the measurement y (i.e., a feature extracted from Lamb wave signals in this study), respectively, and ν is the measurement noise, which is assumed zero-mean Gaussian hereafter.

One main step of the PF routine, and in general of methods for Bayesian inference leveraging on Monte-Carlo sampling, is the drawing of the posterior distribution of the unknown variables, which, in turn, is based on the prior knowledge and the assignment of a score based on the likelihood with respect to the sensor observations. While the selection of the latter is arbitrary (a Gaussian likelihood function is used in this study without any loss of generality), it always entails a comparison between the measurements predicted through the function $g(\cdot)$ and the sensor measurements at discrete time k. However, it rarely happens that the function $g(\cdot)$, calibrated on a set of reference specimens, will properly fit the sensor observations from a different set of specimens, due to the inevitable uncertainties, such as different specimen and damage geometries, sensor errors, etc. Sufficiently large bias between the sensor-based and the predicted measurements will induce inaccurate estimation[18] and prognosis.[7]

This measurement bias can be considered as a typical sensor fault, which can be estimated including a bias parameter in the measurement equation $g(\cdot)$.[20,21] It will have limited effect on the estimation for the other state components when being accurately identified.[22] Therefore, by combing the methods from sensor fault diagnosis and hybrid damage prognosis,[8,17] a new hybrid prognosis model with the bias parameter b included is proposed to improve damage state and parameter estimation in presence of a measurement bias:

$$\begin{cases} \boldsymbol{z}_k = \begin{bmatrix} \boldsymbol{\theta}_k \\ x_k \\ b_k \end{bmatrix} = \begin{bmatrix} \boldsymbol{\theta}_{k-1} + \boldsymbol{\omega}_{\theta,k} \\ f(x_{k-1}, \boldsymbol{\theta}_k, \omega_k) \\ b_{k-1} + \omega_{b,k} \end{bmatrix}, \\ y_k = g(x_k) + b_k + \nu_k \end{cases} \tag{4}$$

where ω_b is the process noise for the parameter b. Note that Equations 3 and 4 are usually nonlinear and non-Gaussian, due to the nonlinear functions $f(\cdot)$ and $g(\cdot)$ and the non-Gaussian noise, respectively, as will be further detailed in Section 3.2.

2.2 | Particle filter

In a Bayesian framework, the unknown state vector at kth step $\boldsymbol{z}_k$ is inferred based on a sequence of sensor observations as follows:

$$p(\boldsymbol{z}_k|\boldsymbol{y}_{1:k-1}) = \int p(\boldsymbol{z}_k|\boldsymbol{z}_{k-1}) p(\boldsymbol{z}_{k-1}|\boldsymbol{y}_{1:k-1}) d\boldsymbol{z}_{k-1}, \tag{5}$$

$$p(\boldsymbol{z}_k|\boldsymbol{y}_{1:k}) \propto p(y_k|\boldsymbol{z}_k) p(\boldsymbol{z}_k|\boldsymbol{y}_{1:k-1}), \tag{6}$$

where $\boldsymbol{y}_{1:k}$ are the measurements collected from time step 1 to k, the transition distribution $p(\boldsymbol{z}_k|\boldsymbol{z}_{k-1})$ and the likelihood function $p(y_k|\boldsymbol{z}_k)$ are obtained from the process and measurement equations, respectively, $p(\boldsymbol{z}_k|\boldsymbol{y}_{1:k-1})$ and $p(\boldsymbol{z}_k|\boldsymbol{y}_{1:k})$ are the prior and the posterior probability distribution functions (PDF) of the variables in the state vector, respectively, and $\propto$ denotes the proportionality.

Equations 5 and 6 form the basis for the optimal Bayesian solution, which is however difficult to be analytically calculated in a nonlinear and non-Gaussian system as it happens in many problems of practical interest. Therefore, the sampling importance resampling (SIR) PF[23] is used in this study to provide an approximated solution for $p(\boldsymbol{z}_k|\boldsymbol{y}_{1:k})$. Figure 2 presents the four steps in SIR PF,[24] i.e.,

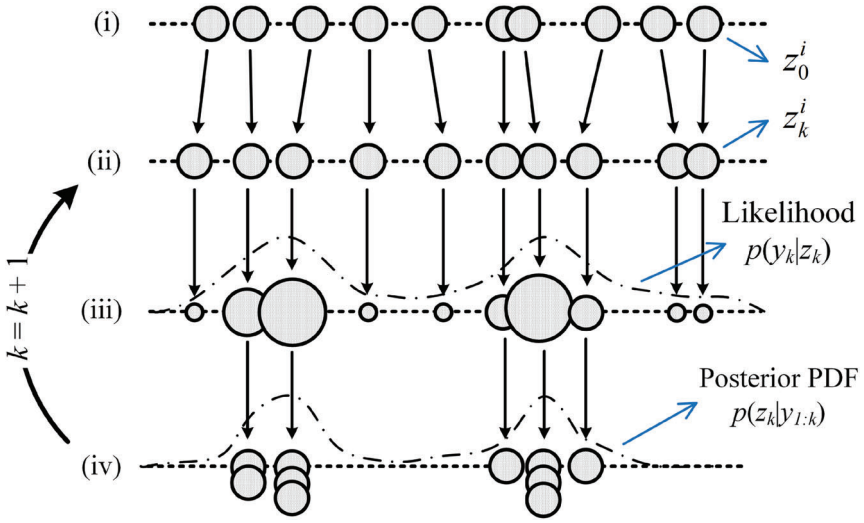

FIGURE 2 Sampling importance resampling (SIR) particle filter[24]

i. **Initialization**: draw N_p particles $\{\boldsymbol{z}_0^i : i = 1,2,...,N_p\}$ from the initial distribution $p(\boldsymbol{z}_0)$,

For $k = 1, 2, ...$

ii. **Prediction:** draw N_p particles $\{\boldsymbol{z}_k^i : i = 1,2,...,N_p\}$ by the transition distribution $p(\boldsymbol{z}_k|\boldsymbol{z}_{k-1})$,

iii. **Updating:** calculate the weight w_k^i by the likelihood function $p(y_k|\boldsymbol{z}_k^i)$ as

$$w_k^i \propto p(y_k|\boldsymbol{z}_k^i), \tag{7}$$

and assign its normalized form $\widetilde{w}_k^i$ to the particle $\boldsymbol{z}_k^i$,

iv. **Resampling** for $\{\boldsymbol{z}_k^i : i = 1,2,...,N_p\}$ using the normalized weights and then assign equal weight to each particle. Systematic resampling is adopted hereafter.

2.3 | Prediction for future state and RUL

The target of many health monitoring applications is that of providing a residual lifetime statistical estimate based on the updated knowledge of the current health state. Thus, by combining the damage evolution model Equation 1 and the kth posterior PDF of damage state $p(x_k|\boldsymbol{y}_{1:k})$, the prognostic step enables predicting the qth step ahead posterior PDF of damage state as follows:[25]

$$p(x_{k+q}|\boldsymbol{y}_{1:k}) = \int \cdots \int \prod_{j=k+1}^{k+q} p(x_j|x_{j-1}) p(x_k|\boldsymbol{y}_{1:k}) \prod_{j=k}^{k+q-1} d(x_j), \tag{8}$$

where $p(x_j|x_{j-1})$ is another form of Equation 1.

Given the impossibility to solve Equation 8 for problems of practical interest, one alternative within a PF framework is to use the particles and their weights to approximate the q-step ahead state PDF as follows:[26]

$$p(x_{k+q}|\boldsymbol{y}_{1:k}) = \sum_{i=1}^{N_p} \widetilde{w}_{k+q-1}^{i} p\left(x_{k+q}|x_{k+q-1}^{i}\right), \tag{9}$$

where $\widetilde{w}_{k+q-1}^{i}$ is the weight of the ith particle at time step $k+q-1$, considered independent from q and equal to $1/N_p$ if particle q-step ahead projection is done after resampling at each iteration. $p\left(x_{k+q}|x_{k+q-1}^{i}\right)$ is computed through Equation 1 and the PF estimates at kth step. Finally, RUL definition requires a damage state threshold to be set l_{th}, thus declaring structural failure when the future damage state calculated by Equation 9 overcomes l_{th}.

Table 1 summarizes the pseudo code for the calculation of the future states and the RUL. The future state evolution of each particle is iteratively calculated through the damage evolution model Equation 1 at each time step k, until the calculated state reaches the threshold l_{th}. The multiplication of the load cycle range (ΔN) and the number of prediction steps ahead is taken as the RUL of each state particle at current time step.

3 | APPLICATION

3.1 | Experimental setup and data

Fatigue tests of a lug joint aluminum specimen, as given in Figure 3, are used to experimentally validate the method. The experimental setup is briefly introduced hereafter and more details can be found in previous studies.[7,17,27] The thickness of the specimen T_s and the diameter of the through-thickness hole D_h are 5 and 25 mm, respectively. A 2-mm notch is machined at the edge of the hole to initiate the fatigue crack growth. The MTS810 electro-hydraulic testing apparatus applies a sinusoidal fatigue load, with maximum load $L_{max} = 18$ kN, corresponding to 25% of the fracture load, load ratio $R = 0.1$ and loading frequency 10 Hz.

A digital microscope is adopted to observe the crack, while 1-mm equally spaced scale lines on the specimen surface allow for target dimension estimate, as presented in Figure 3c. A 1-mm crack length increase is considered each time the crack passes a new line. For better visualization, the fatigue loading is occasionally paused during the test, and an 18-kN static tensile load is applied to the structure to open the crack.

Two piezoelectric transducers are bonded to the surface of the structure for ultrasonics crack monitoring. One serves as the actuator providing an excitation to the structure, while the other is the sensor collecting the Lamb wave signal. During the monitoring process, the crack growth will induce changes in the Lamb wave signals, manifesting as signal delays and peak amplitude modifications, thus also varying the features extracted from the Lamb wave signals and used for crack length assessment.

Five specimens were tested, and their relative crack growths are shown in Figure 4 for specimens labeled S1–S5. It is clear that a deterministic damage evolution model can hardly provide an accurate prognostic result in presence of typical uncertainties related to the material properties, the specimen and test assembling, the external loading condition, etc. As a 1-mm fatigue pre-cracking is performed at the beginning of the fatigue test, the 3-mm crack (the notch

TABLE 1 Calculation of future state and RUL at time step k

Initialization: Set $\{x_k^{i,0} : i = 1,2,...,N_p\}$ as $\{x_k^i : i = 1,2,...,N_p\}$

For $i = 1: N_p$

$q = 0$

While $x_k^{i,q} < l_{th}$

Calculate the future state $x_k^{i,q+1}$ by $x_k^{i,q+1} = f\left(x_k^{i,q}, \boldsymbol{\theta}_k^i\right)$

$q = q + 1$

End

$RUL_k^i = q\Delta N$

End

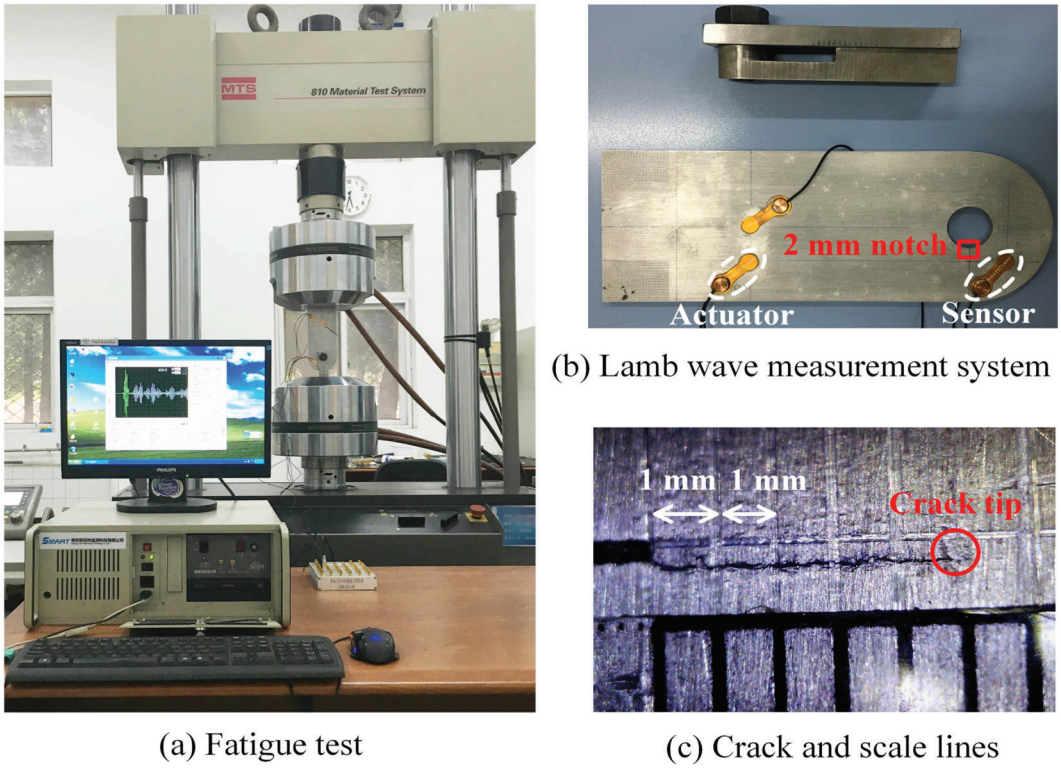

(a) Fatigue test

(b) Lamb wave measurement system

(c) Crack and scale lines

FIGURE 3 Experimental setup[7]

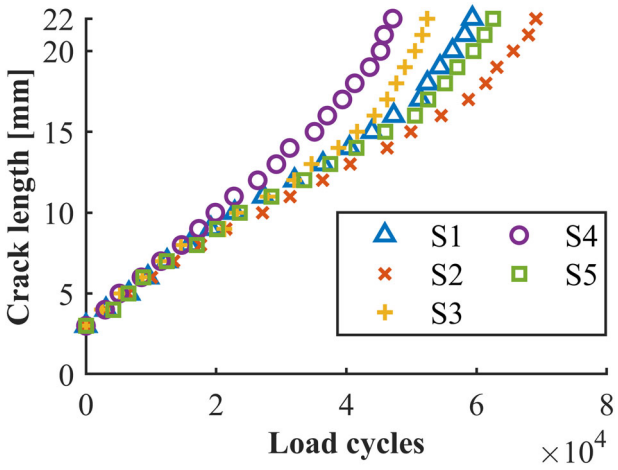

FIGURE 4 Crack growths from specimen S1–S5

length and the pre-cracking length) is taken as the initial crack length, while the threshold crack length for RUL prediction is arbitrarily set to 22 mm, however guaranteeing sufficient residual strength to the joint.

At each measured crack length, the actuator provides a 3-cycle Hanning–Windowed sine burst with central frequency of the excitation 160 kHz, and the sensor collects the Lamb wave signal with the sampling frequency 50 MHz for 2×10^{-4} s, as given in Figure 5. The first wave packet is a crosstalk caused by the electromagnetic induction between the circuits of the actuator and sensor, which carries no information about the crack growth. The signals between 6×10^{-5} and 8×10^{-5} s are taken as the S_0 mode contribution,[7] where the increasing crack length induces a monotonically decreasing amplitude of the signals and a delay of the wave packet as well. These phenomena are used for damage quantification after the feature extraction procedure described below is carried out.

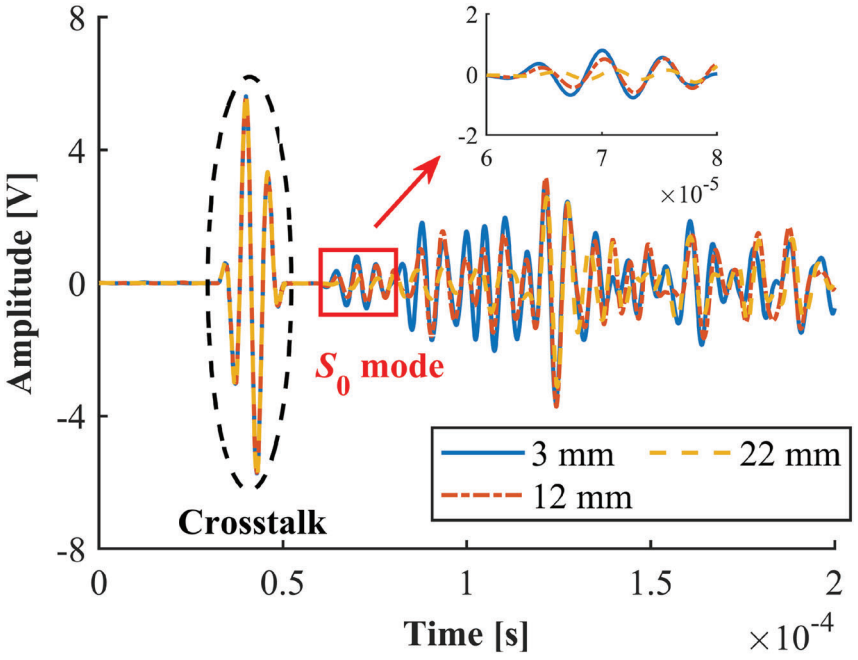

FIGURE 5 Lamb wave signals at three crack lengths from specimen S1

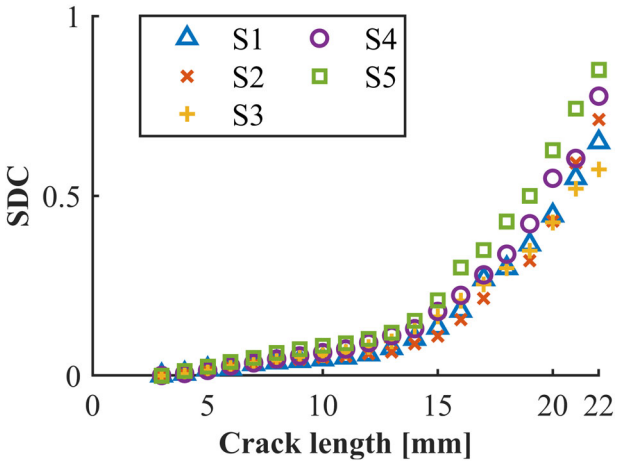

FIGURE 6 SDCs at different crack lengths from specimens S1–S5

The signal difference coefficient (SDC)[28] serves as the statistical feature extracted from the Lamb waves, i.e.:

$$SDC_l = 1 - \left| \frac{cov(f_l, f_b)}{std(f_l)std(f_b)} \right|, \tag{10}$$

where f_b and f_l are the selected S_0 mode signals at the reference crack length 3 mm and current crack length l mm, respectively, the functions "cov" and "std" are the covariance matrix of the two sets of signals and the standard deviation (STD) of one set of signals, respectively. Note that the SDC feature is considered as the available measurement from now on.

Figure 6 presents the monotonically increasing SDCs as a function of crack length for the specimens S1–S5, which confirms the relationship between the crack length and the measurement can vary in different specimens of the same structure. Data relative to specimens S2–S5 are used to fit the function $g(\cdot)$ in the measurement equation in Section 3.2, while specimen S1 will be used for testing the methodology and verify the capability of the algorithm in coping with the bias between the features read in S1 and the corresponding features in S2–S5.

3.2 | Model formulation

The crack growth in a metallic structure subject to fatigue loads is typically described by the Paris' law,

$$\frac{dx}{dN} = C(\Delta K)^m, \tag{11}$$

where x indicates the crack length, C and m are two empirical material parameters governing damage progression, ΔK is the stress intensity factor (SIF) range, calculated with Equation 12 by fitting a set of numerical simulations, as detailed in Appendix A,

$$\Delta K(x) = 0.0014x^3 + 0.5626x^2 - 13.50x + 497.8. \tag{12}$$

With sufficiently small load cycle increment ΔN, Equation 11 can be discretized as

$$x_k = x_{k-1} + C(\Delta K(x_{k-1}))^m \Delta N, \tag{13}$$

and it will be adopted to predict the future crack evolution. The intrinsic stochasticity of the crack growth can be described by adding an unbiased log-normally distributed noise e^{ω} to Equation 13 as in.[3]

$$x_k = x_{k-1} + e^{\omega_k} C(\Delta K(x_{k-1}))^m \Delta N, \tag{14}$$

where $\omega \sim \mathcal{N}\left(-\frac{\sigma^2}{2}, \sigma^2\right)$ is a Gaussian noise with STD σ.

Considering the different crack growth trajectories for the same structure in Figure 4, the future state can hardly be accurately predicted through Equation 13 by considering the parameters in Equation 13 as deterministic and known. One online model updating strategy is to set the parameters C and m as unknown variables and then to form the process equation with both the crack length and parameters included:[3]

$$\begin{bmatrix} \ln C_k \\ m_k \\ x_k \end{bmatrix} = \begin{bmatrix} \ln C_{k-1} + \omega_{1,k} \\ m_{k-1} + \omega_{2,k} \\ x_{k-1} + e^{\omega_k} C_k (\Delta K(x_{k-1}))^{m_k} \Delta N \end{bmatrix}, \tag{15}$$

where ω_1 and ω_2 are zero-mean Gaussian process noises, and $\ln(\cdot)$ is the natural logarithm for an easier sampling.

As the prediction accuracy depends on the state and parameter estimation, kernel smoothing[29] is adopted to improve the estimation performance for the parameters C and m, as already used in.[3,9]

$$\begin{cases} \ln C_k = \sqrt{1-h^2} \ln C_{k-1} + \left(1 - \sqrt{1-h^2}\right) \widehat{\ln C_k} + \omega_{1,k} \\ m_k = \sqrt{1-h^2} m_{k-1} + \left(1 - \sqrt{1-h^2}\right) \widehat{m}_{k-1} + \omega_{2,k} \end{cases}, \tag{16}$$

where $\widehat{\ln C}$ and $\widehat{m}$ denote the means of the samples for the parameters $\ln C$ and m, and $h \in [0\ 1]$ is the smoothing parameter, with a higher value of h meaning a larger shrinkage. The parameter h is set as 0.1, as recommended in Corbetta et al. and Cristiani et al.[3,9]

By combining a measurement equation with Equations 15 and 16, the traditional hybrid prognostic model can finally be formulated as in.[3]

$$\begin{cases} \begin{bmatrix} \ln C_k \\ m_k \\ x_k \end{bmatrix} = \begin{bmatrix} \sqrt{1-h^2} \ln C_{k-1} + \left(1 - \sqrt{1-h^2}\right) \widehat{\ln C_k} + \omega_{1,k} \\ \sqrt{1-h^2} m_{k-1} + \left(1 - \sqrt{1-h^2}\right) \widehat{m}_{k-1} + \omega_{2,k} \\ x_{k-1} + e^{\omega_k} C_k (\Delta K(x_{k-1}))^{m_k} \Delta N \end{bmatrix} \\ y_k = g(x_k) + \nu_k \end{cases}, \tag{17}$$

where the measurement y is the SDC feature obtained from the Lamb waves and the function $g(\cdot)$ describing the mapping between the crack length and the SDC is a fourth-order polynomial function as in.[17]

$$g(x_k) = a_0 {x_k}^4 + a_1 {x_k}^3 + a_2 {x_k}^2 + a_3 x_k + a_4, \tag{18}$$

where a_0, a_1, a_2, a_3, and a_4 are the coefficients obtained from specimens S2—S5 via two steps:

i. the crack lengths and the SDCs for each specimen are fitted by a fourth-order polynomial function to provide one set of coefficients a_0, a_1, a_2, a_3, and a_4 for each specimen;
ii. the averages of the coefficients from the four specimens serve as the corresponding coefficients in $g(\cdot)$.

The new hybrid framework with a bias parameter included for estimation is formulated as

$$\begin{cases} \begin{bmatrix} \ln C_k \\ m_k \\ x_k \\ b_k \end{bmatrix} = \begin{bmatrix} \sqrt{1-h^2}\ln C_{k-1} + \left(1-\sqrt{1-h^2}\right)\widehat{\ln C}_k + \omega_{1,k} \\ \sqrt{1-h^2} m_{k-1} + \left(1-\sqrt{1-h^2}\right)\widehat{m}_{k-1} + \omega_{2,k} \\ x_{k-1} + e^{\omega_k} C_k (\Delta K(x_{k-1}))^{m_k} \Delta N \\ b_{k-1} + \omega_{b,k} \end{bmatrix}, \\ y_k = g(x_k) + b_k + \nu_k \end{cases} \tag{19}$$

where b is the parameter representing the bias, and ω_b is its process noise. Equations 17 and 19 are nonlinear and non-Gaussian, justifying the adoption of the PF algorithm as an efficient state and parameter estimation technique.

3.3 | Target crack growth and SDC observations

The crack length and the Lamb wave feature observations have been experimentally collected at a long interval (i.e., every several thousand load cycles). In order to simulate an online SHM application where the crack length can be evaluated at a shorter interval, exploiting the monotonicity and trendability of the observed features, sequential observations of the target crack growth of specimen S1 have been artificially generated by the following:

i. linearly interpolate the crack length available for specimen S1, generating a new denser target where the crack lengths are available every 300 load cycles,
ii. corrupt the crack lengths by a white Gaussian noise with a signal-to-noise ratio SNR = 50 dB to simulate the uncertainty in crack growth,

iii. use linear interpolation to generate a new SDC at each crack length, and corrupt these SDCs by a white Gaussian noise with SNR = 30 dB to simulate sensor noise.

Figure 7a shows the resulting target crack growth, where a total number of $T = 197$ discrete time steps corresponds to 5.91×10^4 load cycles. Figure 7b shows the sensor-based SDCs and the SDCs predicted by the function $g(\cdot)$ at these crack lengths. A time-varying bias is noticeably existing between the two types of SDCs, potentially hampering the PF performance as shown later in Section 3.5.

3.4 | PF parameters

All the PF parameters used in this study are reported in Table 2. It is worth noting that the PF performance relies on a proper selection of these parameters. The criteria for their selection in this study are given below, while more details on sensitivity analyses can be found in literatures, including number of particles,[30–32] STD in likelihood function,[9] process noise,[30,33] and initial distribution or range.[30]

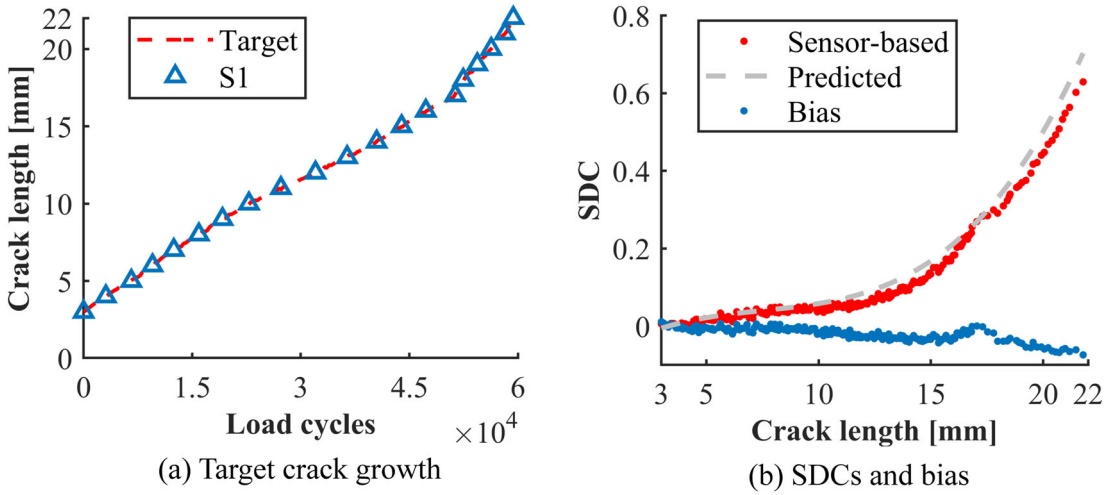

FIGURE 7 Target crack growth and sensor-based and predicted SDCs

TABLE 2 Particle filter parameters

Number of particles N_p		**STD in likelihood function σ_y**	
8,000		**0.01**	
Initial distributions for $\ln C$ $\left[\ln\left(\frac{\text{mm}}{\text{cycle}\left(\text{MPa}\sqrt{\text{mm}}\right)^{-m}}\right)\right]$, m [−]		Initial range for x [mm]	Initial value for b [−]
$\begin{bmatrix}\ln C_0\\ m_0\end{bmatrix} \sim \mathcal{N}\left(\begin{bmatrix}-57.18\\ 8.101\end{bmatrix}, \begin{bmatrix}0.9966 & -0.1764\\ -0.1764 & 0.0346\end{bmatrix}\right)$		$x_0 \in (2.5, 3.5)$	$b_0 = 0$
Distributions of process noises $\{\omega, \omega_1, \omega_2, \omega_3\}$ for x, $\ln C$, m, b			
x, ω [−]	$\ln C$ $\left[\ln\left(\frac{\text{mm}}{\text{cycle}\left(\text{MPa}\sqrt{\text{mm}}\right)^{-m}}\right)\right]$, ω_1 [−]	m, ω_2 [−]	b, ω_3 [−]
$\mathcal{N}\left(-\frac{0.01^2}{2}, 0.01^2\right)$	$\mathcal{N}(0, 0.02^2)$	$\mathcal{N}(0, 0.002^2)$	$\mathcal{N}(0, 0.005^2)$

The number of particles N_p can be set as a trade-off between the accuracy and the computation cost,[34] since PF with more particles generally provides more satisfactory estimates but requires more computational effort.[30–32] A satisfactory number is usually determined through a convergence analysis, meaning particles are increased until no significant improvement is found on the result accuracy.[35–37] Eight thousand particles are sufficient to provide stable estimation results in this study.

The calculation of the particle weights essentially depends on the likelihood of each particle with respect to the actual observation. Given that the measurement noise is assumed zero-mean Gaussian in this study, the likelihood function can be formulated as

$$p\left(y_k|\boldsymbol{z}_k^i\right) = \frac{1}{\sqrt{2\pi}\sigma_y}\exp\left(-\frac{1}{2\sigma_y{}^2}\left(y_k - y_k^i\right)^2\right), \tag{20}$$

where y_k is the observation at kth discrete time step, y_k^i is the simulated observation for the state particle x_k^i, and σ_y can be set as the STD of the measurement noise. However, in different applications, σ_y can be either directly assigned,[5,18,38,39] empirically selected,[40,41] or calculated from the data.[8,42] A trial-and-error procedure is adopted to determine a proper value in this study.

The PF requires the definition of an initial range or distribution for initializing the particles. The initial distributions for $\ln C$ and m in a PF-based damage prognosis framework can be considered as multivariate Gaussian.[3] The means are determined through the fitting procedure in Appendix A, and the covariance matrix are initialized as in Corbetta et al. and Virkler et al.[3,43] All the initial samples of the parameter b are set as zero, as the bias is close to zero at initial step. The initial crack length is set as a range including the initial observed length.

A random term should be included in the process equation to describe the state evolution uncertainty. It does not have to be a physical noise, but it is often referred to as process noise (or system noise), where the "process" and "noise" denote the system evolution process as well as the stochastic and perturbative nature, respectively.[3,44] In implementing the PF, at each time step, N_p process noise samples will be sampled from the distributions in Table 2 and assigned to the N_p particles. The noise distributions in this study are determined from Corbetta et al. and Cristiani et al,[3,9,10] while the means and STDs are selected based on a trial-and-error procedure.

3.5 | Prognostic performances

Figures 8a,b present the crack length and parameter estimation results using the traditional approach without taking the measurement bias into consideration, respectively. Despite that the particles for ln C and m converge around fixed values during the sequential estimation, the estimated crack lengths are noticeably smaller than the true ones during the estimation process. The observed SDCs are smaller than the predicted ones as visible in Figure 7b, meaning those particles underestimating the crack length are assigned larger weights through the likelihood function, and they will be duplicated in the resampling step. The estimated crack lengths after about 5×10^4 load cycles are closer to the target, due to the lower proportion of the bias in the actual measurements. In fact, the ratio of the root mean square (RMS) of the bias with respect to the RMS value of the measurements is 0.11 after about 5×10^4 load cycles, compared to 0.25 before 5×10^4 load cycles. In conclusion, the traditional approach cannot provide an accurate state and parameter estimation, and its performance is highly related to (i) whether the actual measurements are above or below the predicted ones and (ii) the relative magnitude of bias compared to the measurements.

Figures 9a–c present the crack length, material parameters, and bias estimation results by the new approach, respectively. The estimated crack length is noticeably more accurate than that in Figure 8a, as the bias is correctly identified by the PF, and it is taken into consideration for the estimation for the other state components. Both the accurate crack length estimation and the convergence of parameters ln C and m show that the new model can provide more accurate state and parameter estimation results than the traditional model. As the use of one additional parameter in measurement equation introduces additional uncertainties, the confidence boundaries (CBs) for crack length result larger and the particles of the parameters C and m are more diversely distributed, as was also observed in Rabiei et al.[19]

The difficulty in estimating the time-varying bias, which leads to a small-level error in crack length estimation, might be alleviated by (i) adopting PF with an adaptive process noise,[45] which enhance the performance in estimating the time-varying parameter or (ii) collecting the true crack length to update the bias parameter at a limited number of load cycles.

Figures 10a,b present the prediction for future states at 3.6×10^4 load cycles using the traditional and new approaches, respectively. Each gray dotted line is the crack length trajectory predicted by Equation 13 for one posterior

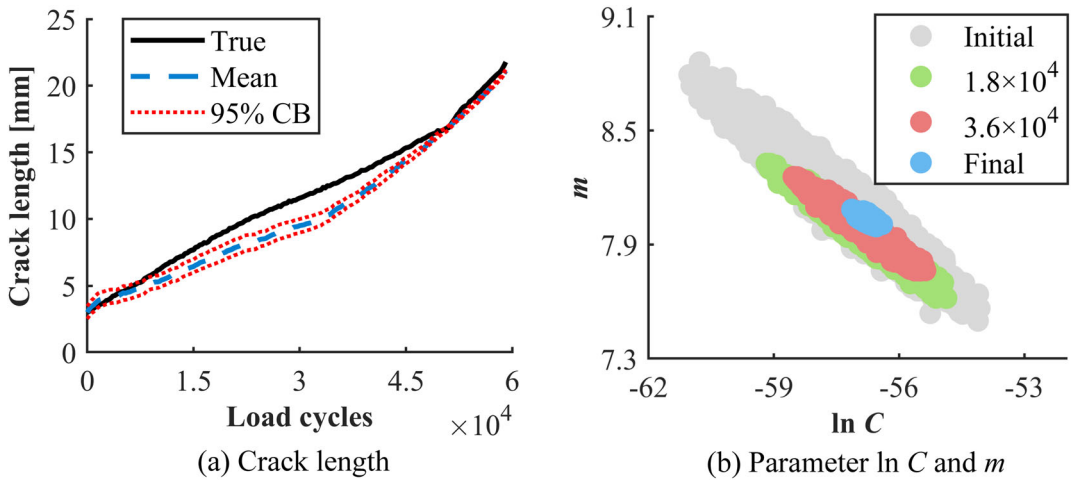

(a) Crack length (b) Parameter ln C and m

FIGURE 8 State and parameter estimation using traditional model

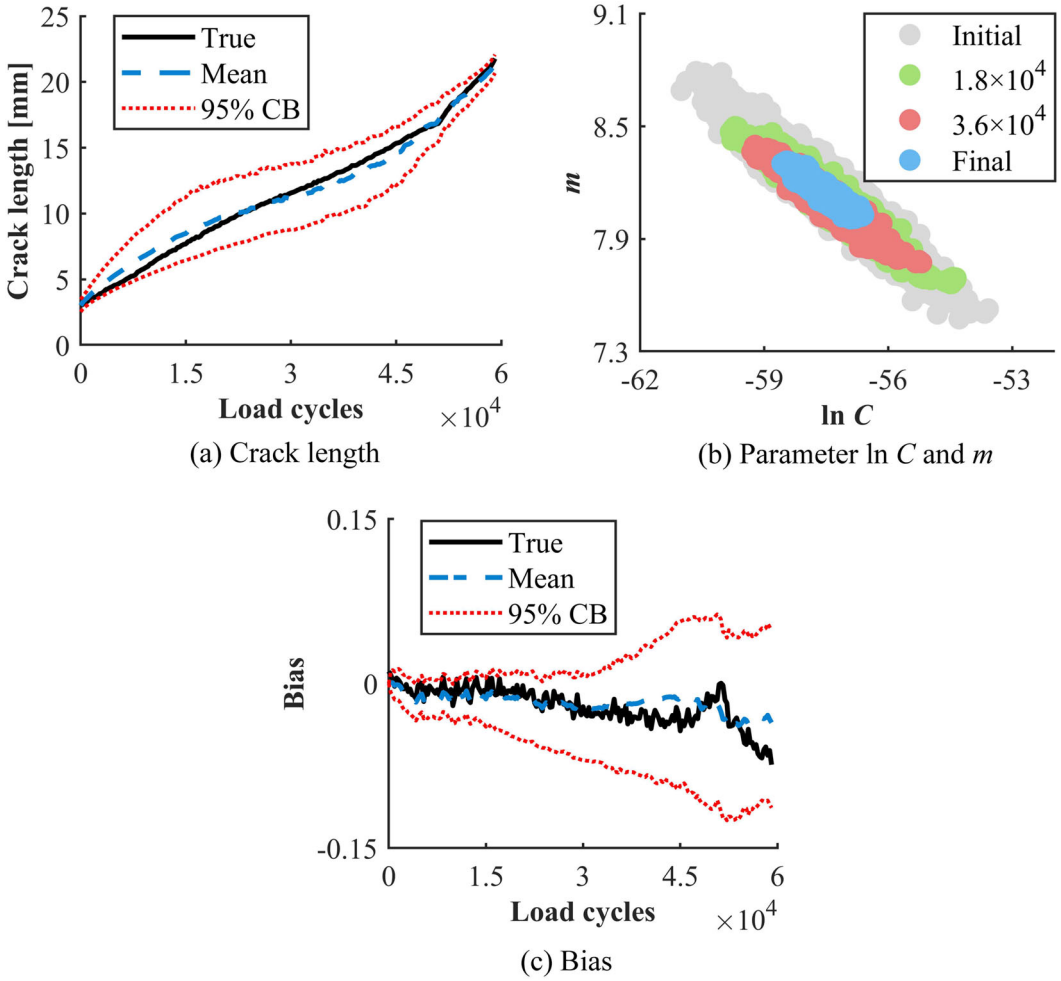

FIGURE 9 State and parameter estimation using new model

sample of the state vector. The gray histogram at the end of life (identified as the critical crack length 22 mm) is the RUL posterior PDF. Figures 11a,b show the RUL predictions using the traditional and new approaches, respectively, along with their 95% CBs. The predicted states and the RUL are noticeably improved by adding the bias as a parameter to be estimated in the state vector, which is strictly related to the improved accuracy of the state posterior estimates.

3.6 | Performances under different-magnitude biases

The performance of the two approaches (with and without taking the bias into consideration) is now tested under different-magnitude biases. Four sets of SDCs target observations are artificially created by

i. scaling the bias in Figure 7b (without measurement noise) by a set of scaling factors s_f {0, 0.5, 1.5, 2} to create four bias levels with the same morphology,
ii. adding these biases to the predicted SDCs in Figure 7b, and

iii. corrupting the artificially generated SDCs observations by a white Gaussian noise with SNR 30 dB.

The analysis in Section 3.5 is repeated with the four sets of SDCs. Performances are expressed in terms of the root mean square errors (RMSEs) metric for the crack length and bias, while the cumulative relative accuracy (CRA) metric is used for the RUL:

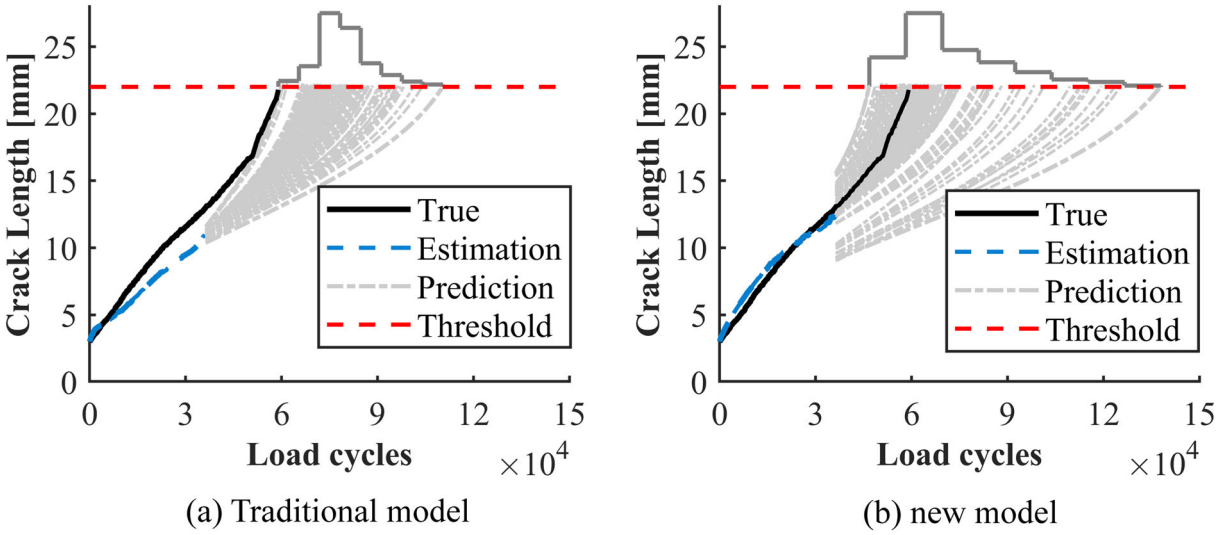

FIGURE 10 Predicted future states at 3.6×10^4 load cycles from traditional and new models

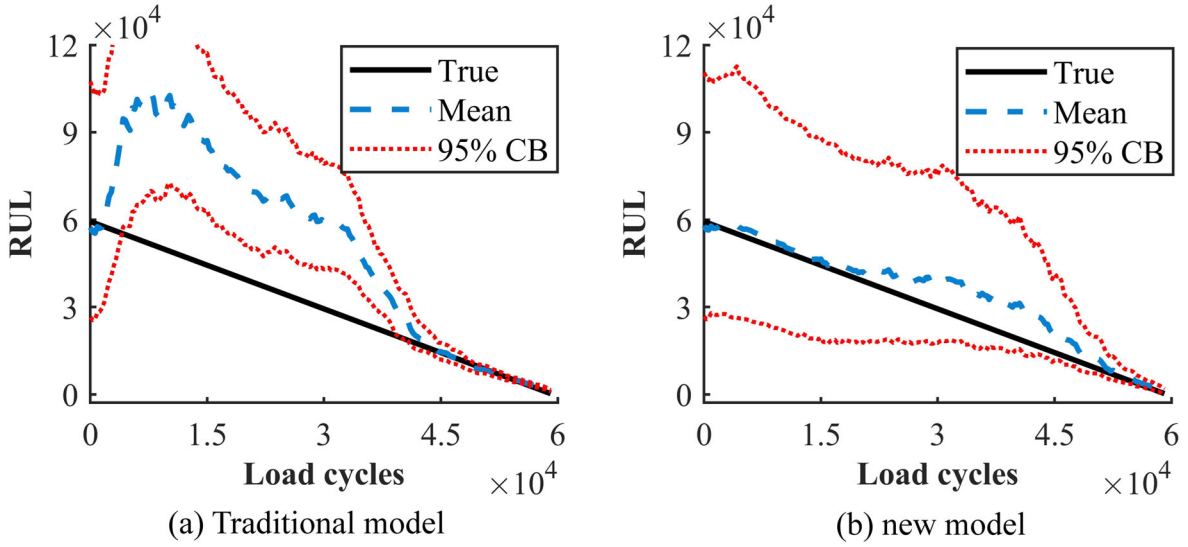

FIGURE 11 RUL predictions from traditional and new models

$$RMSE = \sqrt{\frac{1}{T}\sum_{k=1}^{T}\left(s_{mean,k} - s_{true,k}\right)^2}, \tag{21}$$

$$CRA = \sum_{k=1}^{T-1}\left(1 - \frac{\left|RUL_{mean,k} - RUL_{true,k}\right|}{RUL_{true,k}}\right), \tag{22}$$

where s is the generic state component to be evaluated, either the crack length or the bias, and $T = 197$ is the number of discrete time steps. Lower RMSE and higher CRA represent better estimation and prognosis performances, respectively.

Figures 12a–c present the RMSEs of crack length, the CRAs of RUL, and the RMSE of bias, respectively, as a function of the level of bias. Note that the results of the level-one magnitude have already been presented in Section 3.5. The traditional approach slightly outperforms the new approach under no bias, because the unnecessary bias

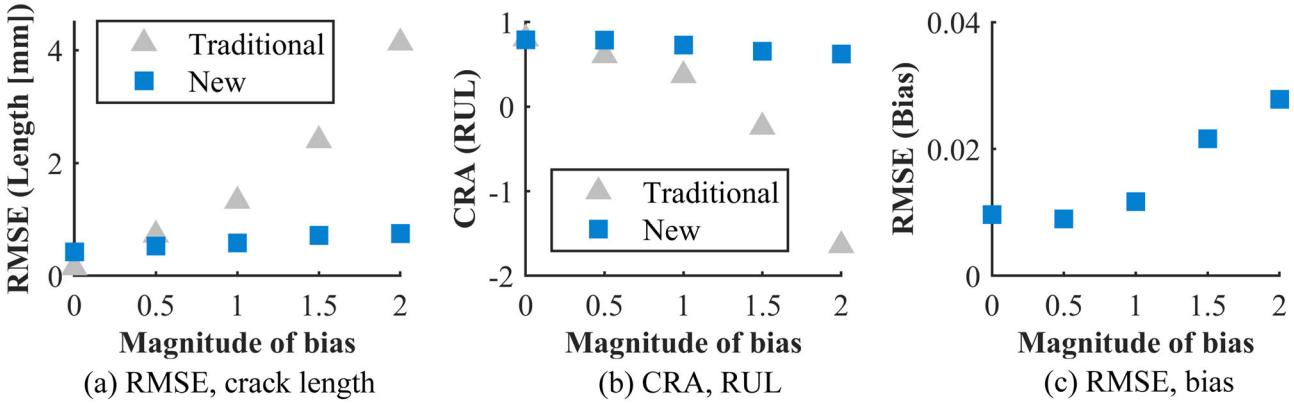

FIGURE 12 Performances of the traditional and new models under different-magnitude biases

estimation introduces more uncertainties. By increasing the bias level, the estimation and prognostic performances of the traditional model significantly decrease, compared with the slight decrease of new model. Meanwhile, the latter might be difficult to be avoided in practice, because the larger the bias level is, the less accurate its estimation will be, as given in Figure 12c, but this might be alleviated resorting to the two strategies mentioned Section 3.5, i.e., (i) adopting a more efficient state estimation technique, e.g., the adaptive PF,[45] to estimate the time-varying bias parameter, and (ii) collecting the true crack length to update the bias parameter at some load cycles.

4 | CONCLUSIONS

The bias between the sensor observation and its prediction by a measurement equation is unavoidable in hybrid prognostic investigations, leading to inaccurate state and parameter estimations and prognostic results. Inspired by sensor fault diagnosis and hybrid damage prognosis, this paper has proposed a new hybrid state space model that includes a bias parameter in the prognostic model for estimation. The experimental study, where an aluminum lug structure is subject to fatigue cracking and monitored by ultrasonic Lamb waves, has proven that the new model can provide accurate estimation and prognostic results provided that the bias is correctly estimated. Furthermore, the estimation and prognostic performances of the new approach have been shown to be noticeably more robust than those of the traditional model in presence of an increasing bias. The slight performance reduction by increasing the bias level might not be avoided even in the newly proposed approach, but can be alleviated by combining different features for damage quantification or by implementing an efficient state estimation technique for time-varying parameters.

The approach remains valid for more complex scenarios, although the acquisition of sufficient experimental or in-field data during the entire run-to-failure process might be infeasible, due to unconceivable costs. Thus, one may resort to simulated data, e.g. from a finite element model, for the definition of the measurement model and the process equation, surely affected by bias, thus justifying additional effort by the authors in present and future research. Moreover, with tens or hundreds of sensors installed on large structures, the measurement equation will become high-dimensional. Although most of the measurements will be unaffected by damage, due to its localized nature, this may lead to an inaccurate and time-consuming prognosis. Online selection of the most appropriate combination of observations is another promising field of research in this framework.

ACKNOWLEDGMENTS

This project has received funding from the European Union's Horizon 2020 research and innovation programme under the Marie Skłodowska-Curie grant agreement no. 859957.

DATA AVAILABILITY STATEMENT

The data that support the findings of this study are available on request from the corresponding author. The data are not publicly available due to privacy or ethical restrictions.

ORCID

Claudio Sbarufatti https://orcid.org/0000-0001-5511-8194
Francesco Cadini https://orcid.org/0000-0001-9235-396X

REFERENCES

1. Chiachío J, Chiachío M, Sankararaman S, Saxena A, Goebel K. Condition-based prediction of time-dependent reliability in composites. *Reliability Engineering & System Safety*. 2015;142:134-147.
2. Chiachío M, Chiachío J, Sankararaman S, Goebel K, Andrews J. A new algorithm for prognostics using Subset Simulation. *Reliability Engineering & System Safety*. 2017;168:189-199.
3. Corbetta M, Sbarufatti C, Giglio M, Todd MD. Optimization of nonlinear, non-Gaussian Bayesian filtering for diagnosis and prognosis of monotonic degradation processes. *Mechanical Systems and Signal Processing*. 2018;104:305-322.
4. Cadini F, Sbarufatti C, Corbetta M, Cancelliere F, Giglio M. Particle filtering-based adaptive training of neural networks for real-time structural damage diagnosis and prognosis. *Struct Control Health Monit*. 2019;26(12).
5. Chiachío J, Jalón ML, Chiachío M, Kolios A. A Markov chains prognostics framework for complex degradation processes. *Reliability Engineering & System Safety*. 2020;195:106621.
6. Guo L, Li N, Jia F, Lei Y, Lin J. A recurrent neural network based health indicator for remaining useful life prediction of bearings. *Neurocomputing*. 2017;240:98-109.
7. Chen J, Yuan S, Wang H. On-line updating Gaussian process measurement model for crack prognosis using the particle filter. *Mechanical Systems and Signal Processing*. 2020;140:106646.
8. Chen J, Yuan S, Jin X. On-line prognosis of fatigue cracking via a regularized particle filter and guided wave monitoring. *Mechanical Systems and Signal Processing*. 2019;131:1-17.
9. Cristiani D, Sbarufatti C, Giglio M. Damage diagnosis and prognosis in composite double cantilever beam coupons by particle filtering and surrogate modelling. *Structural Health Monitoring*. 2020;1475921720960067.
10. Cristiani D, Sbarufatti C, Cadini F, Giglio M. Fatigue damage diagnosis and prognosis of an aeronautical structure based on surrogate modelling and particle filter. *Structural Health Monitoring*. 2020;1475921720971551.
11. Orchard ME, Vachtsevanos GJ. A particle-filtering approach for on-line fault diagnosis and failure prognosis. *Transactions of the Institute of Measurement and Control*. 2009;31(3-4):221-246.
12. Peng Y, Dong M, Zuo MJ. Current status of machine prognostics in condition-based maintenance: a review. *The International Journal of Advanced Manufacturing Technology*. 2010;50(1-4):297-313.
13. Liao L, Köttig F. Review of hybrid prognostics approaches for remaining useful life prediction of engineered systems, and an application to battery life prediction. *IEEE Transactions on Reliability*. 2014;63(1):191-207.
14. Lei Y, Li N, Guo L, Li N, Yan T, Lin J. Machinery health prognostics: A systematic review from data acquisition to RUL prediction. *Mechanical Systems and Signal Processing*. 2018;104:799-834.
15. Lopez I, Sarigul-Klijn N. A review of uncertainty in flight vehicle structural damage monitoring, diagnosis and control: Challenges and opportunities. *Progress in Aerospace Sciences*. 2010;46(7):247-273.
16. Baraldi P, Mangili F, Zio E. Investigation of uncertainty treatment capability of model-based and data-driven prognostic methods using simulated data. *Reliability Engineering & System Safety*. 2013;112:94-108.
17. Yuan S, Chen J, Yang W, Qiu L. On-line crack prognosis in attachment lug using Lamb wave-deterministic resampling particle filter-based method. *Smart Materials and Structures*. 2017;26(8):085016.
18. Cadini F, Sbarufatti C, Corbetta M, Giglio M. A particle filter-based model selection algorithm for fatigue damage identification on aeronautical structures. *Structural Control & Health Monitoring*. 2017;24(11):e2002.
19. Rabiei E, Droguett EL, Modarres M. Fully adaptive particle filtering algorithm for damage diagnosis and prognosis. *Entropy*. 2018;20(2).
20. Giremus A, Tourneret J-Y, Calmettes V. A particle filtering approach for joint detection/estimation of multipath effects on GPS measurements. *IEEE Transactions on Signal Processing*. 2007;55(4):1275-1285.
21. Grauer JA. Real-Time Data-Compatibility Analysis Using Output-Error Parameter Estimation. *J Aircr*. 2015;52(3):940-947.
22. An D, Choi J-H, Kim NH. Identification of correlated damage parameters under noise and bias using Bayesian inference. *Structural Health Monitoring*. 2011;11:293-303.
23. Arulampalam MS, Maskell S, Gordon N, Clapp T. A tutorial on particle filters for online nonlinear/non-Gaussian Bayesian tracking. *IEEE Transactions on Signal Processing*. 2002;50(2):174-188.
24. Chatzi EN, Smyth AW. Particle filter scheme with mutation for the estimation of time-invariant parameters in structural health monitoring applications. *Structural Control & Health Monitoring*. 2013;20(7):1081-1095.
25. Doucet A, Godsill S, Andrieu C. On sequential Monte Carlo sampling methods for Bayesian filtering. *Statistics & Computing*. 2000;10(3):197-208.
26. Zio E, Peloni G. Particle filtering prognostic estimation of the remaining useful life of nonlinear components. *Reliability Engineering & System Safety*. 2011;96(3):403-409.
27. Chen J, Yuan S, Qiu L, Wang H, Yang W. On-line prognosis of fatigue crack propagation based on Gaussian weight-mixture proposal particle filter. *Ultrasonics*. 2017;82:134-144.
28. Qing XP, Chan H-L, Beard SJ, Kumar A. An active diagnostic system for structural health monitoring of rocket engines. *Journal of Intelligent Material Systems and Structures*. 2006;17(7):619-628.

29. Liu J, West M. Combined parameter and state estimation in simulation-based filtering, sequential Monte Carlo methods in practice. *Springer*. 2001;197-223.
30. Chatzi EN, Smyth AW. The unscented Kalman filter and particle filter methods for nonlinear structural system identification with non-collocated heterogeneous sensing. *Structural Control & Health Monitoring*. 2010;16:99-123.
31. Ubeda-Medina L, García-Fernández A, Grajal J. Sigma-point multiple particle filtering. *Signal Processing*. 2019;160:271-283.
32. Chavali P, Nehorai A. Hierarchical particle filtering for multi-modal data fusion with application to multiple-target tracking ☆. *Signal Processing*. 2014;97:207-220.
33. Yoo SJ, Jung DH, Kim JH, Lee JM. A comparative study of soft sensor design for lipid estimation of microalgal photobioreactor system with experimental validation. *Bioresour Technol*. 2015;179:275-283.
34. Li X, Yang X, Yang Y, Bennett I, Mba D. An intelligent diagnostic and prognostic framework for large-scale rotating machinery in the presence of scarce failure data. *Struct Health Moni*. 2019;5:1375-1390, 1475921719884019.
35. Nguyen LH, Goulet J-A. Real-time anomaly detection with Bayesian dynamic linear models. *Struct Control Health Monit*. 2019;26(9): e2404.
36. Ching J, Beck JL, Porter KA. Bayesian state and parameter estimation of uncertain dynamical systems. *Probabilistic Engineering Mechanics*. 2006;21(1):81-96.
37. Sen D, Erazo K, Nagarajaiah S. Bayesian estimation of acoustic emissions source in plate structures using particle-based stochastic filtering. *Struct Control Health Monit*. 2017;24(11):e2005.
38. Fan X, Liu Y. Use of monitored daily extreme stress data for performance prediction of steel bridges: Dynamic linear models and Gaussian mixed particle filter. *Mechanical Systems and Signal Processing*. 2019;121:841-855.
39. Cadini F, Zio E, Peloni G. Particle filtering for the detection of fault onset time in hybrid dynamic systems with autonomous transitions. *IEEE Transactions on Reliability*. 2012;61(1):130-139.
40. Chen C, Zhang B, Vachtsevanos G, Orchard M. Machine condition prediction based on adaptive neuro–fuzzy and high-order particle filtering. *IEEE Transactions on Industrial Electronics*. 2011;58(9):4353-4364.
41. Corbetta M, Sbarufatti C, Giglio M, Saxena A, Goebel K. A Bayesian framework for fatigue life prediction of composite laminates under co-existing matrix cracks and delamination. *Composite Structures*. 2018;187:58-70.
42. Sajeeb R, Manohar CS, Roy D. A conditionally linearized Monte Carlo filter in non-linear structural dynamics. *International Journal of Non-Linear Mechanics*. 2009;44(7):776-790.
43. Virkler DA, Hillberry BM, Goel PK. The statistical nature of fatigue crack propagation. *Journal of Engineering Materials and Technology*. 1979;101(2):148-153.
44. Svensson A, Schön TB, Lindsten F. Learning of state-space models with highly informative observations: a tempered sequential Monte Carlo solution. *Mechanical Systems and Signal Processing*. 2018;104:915-928.
45. Liu M, Zang S, Zhou D. Fast leak detection and location of gas pipelines based on an adaptive particle filter. *International Journal of Applied Mathematics & Computer Science*. 2005;15:541-550.

How to cite this article: Li T, Sbarufatti C, Cadini F, Chen J, Yuan S. Particle filter-based hybrid damage prognosis considering measurement bias. *Struct Control Health Monit*. 2021;e2914. doi:10.1002/stc.2914

APPENDIX A.

Given the analytical solution for the SIFs at different crack lengths is not available, numerical models of the lug structure are built by ABAQUS to provide the maximum SIFs K_{max} at several crack lengths under the maximum fatigue load, which are then used to establish the relationship between the SIF range ΔK and the crack length. The numerical model is plotted in Figure A1.

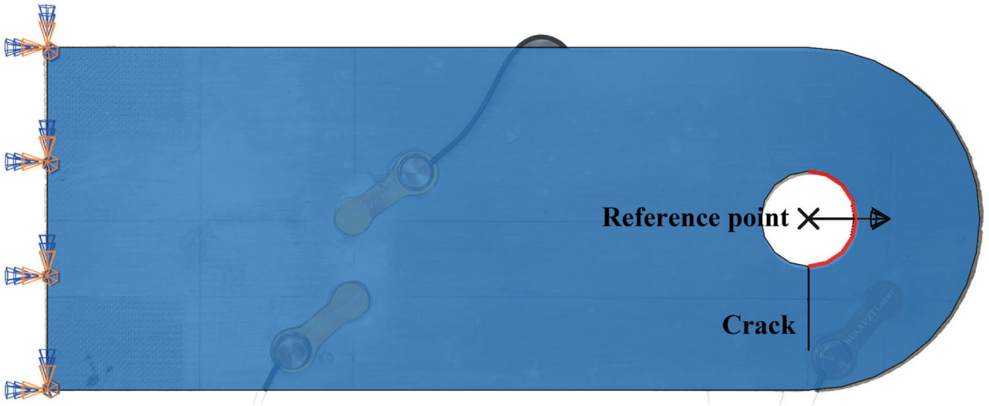

FIGURE A1 ABAQUS model of the experimental structure

The lug structure is modeled as a 2D shell, with Young's modulus, density and Poisson's ratio 72,000 MPa, 2,700 kg/dm^3, and 0.33, respectively. The left side of the structure is fixed. A reference point is located at the center of the circle hole, and it is coupling with the right side of the hole (plotted as red curve). The static analysis, where a concentrated force (maximum fatigue load, 18 kN) is horizontally applied to the reference point, is used to provide the SIF K_{max} at each crack length.

Table A1 lists the numerical SIFs at different crack lengths. Considering that no nonlinearity exists in this model, the SIF range ΔK at each crack length can be calculated by the K_{max} and the load ratio R. A third order polynomial regression is used to fit the relationship between the crack length x and SIF range ΔK. Specifically, Equation 13 can be transformed into its logarithmic form:

$$\underbrace{\ln\frac{x_k - x_{k-1}}{\Delta N}}_{Output} = \ln C + m\underbrace{\ln \Delta K(x_{k-1})}_{Input}, \tag{A1}$$

where $\ln C$ and m can be easily calculated by the input and output (with x_k and x_{k-1} being two observed consecutive crack lengths) from specimens S2–S5 through a first order polynomial fitting regression. They result -57.18 $\left[\ln\left(\frac{\text{mm}}{\text{cycle}\left(\text{MPa}\sqrt{\text{mm}}\right)^{-m}}\right)\right]$ and 8.101 $[-]$, respectively, and are considered for the initialization of the multivariate Gaussian distribution for $\ln C$ and m.

TABLE A1 Polynomial regression using numerical SIF ranges at different crack lengths

Crack length x [mm]	**3**	**5**	**8**	**10**	**12**	**15**	**18**	**20**	**22**
K_{max} $[MPa\cdot\sqrt{mm}]$	514.4	493.3	473.2	467.4	466.7	475.0	494.3	514.7	543.5
ΔK $[MPa\cdot\sqrt{mm}]$	$K_{max}(1-R)$								
Third order polynomial regression: $\Delta K(x) = 0.0014x^3 + 0.5626x^2 - 13.50x + 497.8$									